Effect of TiO_2 addition on structure, solubility and crystallisation of phosphate invert glasses for biomedical applications

Delia S. Brauer[1,2,*], Natalia Karpukhina[3], Robert V. Law[3], Robert G. Hill[2]

[1]Imperial College, Department of Materials, Exhibition Road, London SW7 2AZ, UK

[2]Barts and The London, Unit of Dental Physical Sciences, Mile End Road, London E1 4NS, UK

[3]Imperial College, Department of Chemistry, Exhibition Road, London SW7 2AZ, UK

*Corresponding author. Tel.: +44 (0)207 882 7409; fax: +44 (0)207 882 7979. *E-mail address*: d.brauer@qmul.ac.uk.

Abstract

Phosphate invert glasses in the system P_2O_5-CaO-MgO-Na_2O are completely soluble and exhibit a neutral pH in aqueous media and they are therefore of interest for use as degradable implant materials. Their structure consists of small phosphate units such as pyrophosphate ($P_2O_7^{4-}$) and hence they are prone to crystallisation. Addition of TiO_2 is known to improve processing of the melt and also to control glass solubility. We investigated the glass structure of phosphate glasses with 37 and 35 mol% P_2O_5 and addition of 1 to 10 mol% TiO_2 and how structural changes influenced solubility, thermal properties, processing window and crystallisation behaviour. Glasses showed an increase in activation energy for crystallisation with increasing TiO_2 content, resulting in an increased processing window and thereby allowing for fibre drawing and sintering of porous scaffolds. Deconvolution of ^{31}P MAS NMR and calculation of network connectivity and average chain lengths suggest that Ti is acting as a network modifier with Ti^{4+} units acting as ionic crosslinks between phosphate units thereby impeding crystallisation as well as chain hydration and subsequent chain dissolution.

PACS

61.05.cp, 61.43.Fs, 64.75.Bc, 65.60.+a, 81.05.Kf, 82.56.Ub, 87.85.J-

Keywords

MAS-NMR, Structure, X-ray diffraction, Thermal properties, Biomaterials B124, Dissolution D228; Phosphate glasses P147

1. Introduction

Phosphate glasses in the system P_2O_5-CaO-MgO-Na_2O dissolve completely in aqueous solutions and they have a composition similar to that of the mineral phase of bone, which makes them interesting materials for degradable implants. Structure and properties of phosphate glasses strongly depend on the phosphate content, and phosphate glasses can be divided into three groups corresponding to their phosphate content and structure: Ultraphosphate glasses contain more than 50 mol% P_2O_5, they exhibit a phosphate network glass structure consisting of Q^3 structural units and give an acidic pH in water. Polyphosphate glasses contain 50 mol% P_2O_5 or less. At 50 mol% P_2O_5 (metaphosphate composition) they consist of phosphate Q^2 chains of in theory infinite length with the chain length decreasing for decreasing phosphate content. At 33 mol% P_2O_5 (pyrophosphate stoichiometry) the glass structure consists of $P_2O_7^{4-}$ units, *i.e*. Q^1 dimers, while for 25 mol% P_2O_5 or less only orthophosphate (Q^0) groups are present [1].

Phosphate glasses containing less than 40 mol% P_2O_5 are often referred to as invert glasses, as their properties depend on the network modifier ions rather than on the network former [1]. These glasses degrade more slowly than compositions in the meta- or ultraphosphate region [2-4]. Their structure is highly disrupted and consists of small phosphate units such as pyrophosphate or orthophosphate groups, and therefore these glasses are prone to crystallisation. This makes processing difficult and stabilisation is desirable. Processing of phosphate invert glasses can be successfully improved by addition of TiO_2 [5-7]. In addition, the only phosphate glass shown to form an apatite layer in simulated body fluid *in vitro* was a TiO_2-containing invert glass [5], and this apatite layer is generally thought to facilitate attachment of osteoblasts *in vivo*, thereby allowing for the formation of an intimate bond to bone [8].

Aim of our work was to investigate how addition of TiO_2 influences glass structure and crystallisation behaviour in the system P_2O_5-CaO-MgO-Na_2O with phosphate contents of 37 and 35 mol%.

2. Materials & Methods

2.1 Glass synthesis

Phosphate invert glasses in the system P_2O_5-CaO-MgO-Na_2O-TiO_2 were produced using a melt quench route as described earlier [4]. Synthetic glass composition is given in Table 1. For glasses A to D TiO_2 was added in increasing amounts (1 to 10 mol%) while P_2O_5 content was kept at 37 mol% and the ratio CaO:MgO:Na_2O was kept constant. An additional glass (E) was produced with a lower phosphate content (35 mol%). Glass monoliths were produced by quenching the melt between copper blocks to prevent surface crystallisation and subsequent annealing at glass transition temperature (T_g).

Table 1: Synthetic (top) and analytic (bottom) glass composition in mol% (95% confidence interval).

Glass	P_2O_5	CaO	MgO	Na_2O	TiO_2
A	37.0	29.0	10.0	24.0	-
	36.93 (0.74)	29.39 (0.21)	10.05 (0.13)	23.63 (0.30)	-
B	37.0	28.6	9.8	23.6	1.0
	36.88 (0.75)	29.37 (0.22)	9.91 (0.13)	22.73 (0.31)	1.11 (0.13)
C	37.0	26.7	9.2	22.1	5.0
	nm	nm	nm	nm	nm
D	37.0	24.4	8.4	20.2	10.0
	nm	nm	nm	nm	nm
E	35.0	27.5	9.5	22.5	5.5
	34.04 (0.76)	28.84 (0.22)	10.48 (0.14)	20.86 (0.31)	5.78 (0.13)

nm = not measured

2.2 Glass characterisation

Glass frit was ground to powder in a vibratory mill (Gyro Mill, Glen Creston, UK). Powder X-ray diffraction (XRD; PANalytical, X'Pert PRO MPD, 40 kV, 40 mA, Cu*K*α, data collected at room temperature) was performed to confirm the amorphous structure of the quenched glass. For chemical analysis of the glass composition, the glasses were dissolved in 37% hydrochloric acid (HCl) and analyzed using inductively coupled plasma with optical emission spectroscopy (ICP-OES). Glass solubility in deionised water was investigated and analysed using ICP-OES as described earlier [4]. Temperature behaviour was investigated by differential scanning calorimetry (DSC) using both glass frit and milled glass powder. The glass transition temperature (T_g) was determined as the onset temperature of the transition temperature range. The processing window was calculated as the difference between crystallisation onset ($T_{c,ons}$) and T_g. From DSC traces obtained using different heating rates (5, 10, 15, 20 and 25 K/min) activation energies (E_a) for T_g and crystallisation were calculated [9].

Milled glass powder was heat-treated in analogous fashion to the DSC experiments: The samples were heated to $T_{c,ons}$ at a heating rate of 10 K/min and then were allowed to cool to room temperature without holding at $T_{c,ons}$. Crystal phases were analysed using XRD and NMR (cf. below).

2.3 Structural investigation

Glass structure was investigated using Raman spectroscopy and ^{31}P MAS NMR. Raman spectra were obtained using glass monoliths at Raman shifts between 500 and 1500 cm^{-1} (Renishaw RM 2000 connected to Leica Microscope with 50× objective). ^{31}P MAS NMR spectra were acquired at 81.0 MHz in the 4 mm rotor spinning at 4.5 kHz (Bruker 200 MHz (4.7 T) spectrometer). 64 transients of a single pulse experiment with 2.5 μs π/2 pulse and 49 s recycle delay were collected for each sample. ^{31}P chemical shift was referenced to the signal of 85% H_3PO_4. For deconvolution of ^{31}P MAS NMR of glass samples, dmfit software was used [10].

Network connectivity (NC) is defined as the number of bridging oxygens (BO) per network forming element [11]. Theoretical network connectivity was calculated according to

$$NC_{theor} = \frac{[P_2O_5] - [M_2^{I}O] - [M^{II}O] - 2[M^{IV}O_2]}{[P_2O_5]}$$

where $[M_2^{I}O]$, $[M^{II}O]$ and $[M^{IV}O_2]$ are the molar fractions of the network modifiers and $[P_2O_5]$ is the molar fraction of phosphate. Theoretical average chain length ($\overline{n}_{theor}$) was calculated according to Bunker [12] with

$$\overline{n}_{theor} = \frac{2}{\frac{[M_2^{I}O]+[M^{II}O]+2[M^{IV}O_2]}{[P_2O_5]} - 1}$$

3. Results

3.1 Chemical analysis and dissolution

All compositions were obtained in a glassy state with the amorphous structure being confirmed by XRD (not shown) and NMR (see below). Chemical analyses of the glasses A, B and E reveal that differences between nominal and analysed glass compositions are negligible (Table 1). Glass solubility in deionised water decreased significantly with increasing TiO_2 content (Fig. 1). Ratio of modifier ions (CaO, MgO, Na_2O, TiO_2) to P_2O_5 in dissolved ions increases with increasing TiO_2 content in the glass (Fig. 2a), which means that the relative amount of phosphate in the dissolved oxides decreases. Fig. 2b shows a decrease in the absolute amounts of dissolved P_2O_5, CaO, MgO and Na_2O, while the absolute amount of dissolved TiO_2 increases.

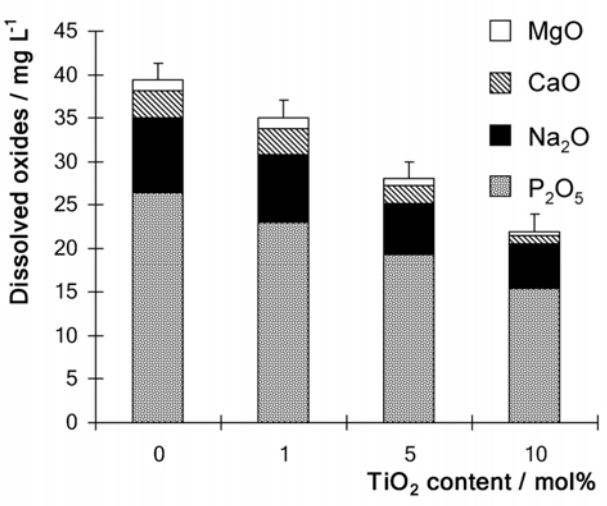

Figure 1: Glass solubility in deionised water at 98°C analysed using ICP-OES. (Error bars show the 95% confidence interval.)

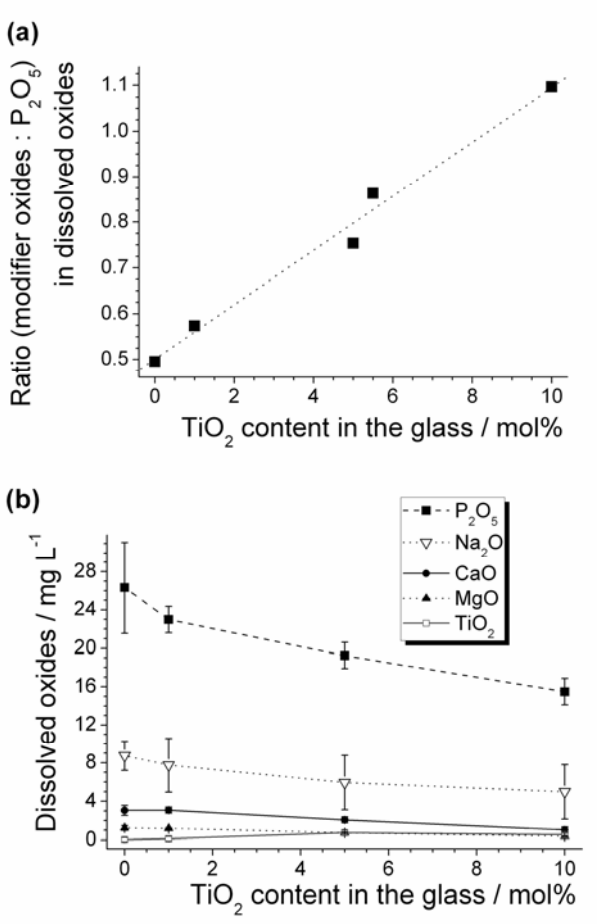

Figure 2: (a) Ratio of network modifier oxides (CaO, MgO, Na_2O, TiO_2) to P_2O_5 in dissolved ions. Dotted line represents linear regression of data for glasses A to E (Regression coefficient: R = 0. 993), (b) dissolved ions calculated as oxides *vs*. TiO_2 content in the glass. (Lines are drawn as a guide to the eye.)

3.2 Temperature behaviour

Table 2 shows DSC results for milled glass powder and frit. DSC results for glass frit show an increase in T_g, $T_{c,ons}$ and crystallisation peak temperature ($T_{c,pk}$) with increasing TiO_2 content (glasses A – D; Fig. 3). However, when using milled glass powder, values for the TiO_2-free glass A were slightly higher than those of glass B (1 mol%, Table 2, values in brackets). The processing window (*i.e.*, the temperature range between T_g and $T_{c,ons}$) increases linearly with increasing TiO_2 content when the P_2O_5 content is kept constant (glasses A – D, Fig. 4) from 132 K (TiO_2-free glass A) to 183 K (glass D, 10 mol% TiO_2).

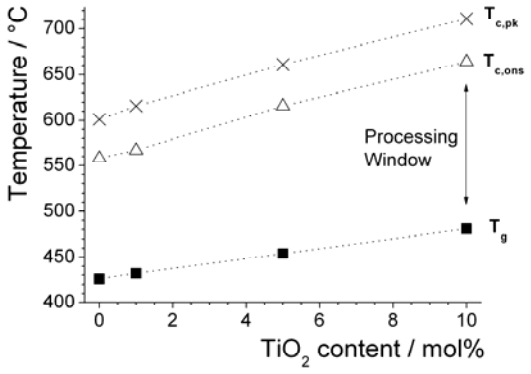

Figure 3: T_g, $T_{c,ons}$ and $T_{c,pk}$ vs. TiO_2 content in mol% for glasses A to D (results obtained using glass frit). The error is less than the size of the symbols. (Lines are drawn as a guide to the eye.)

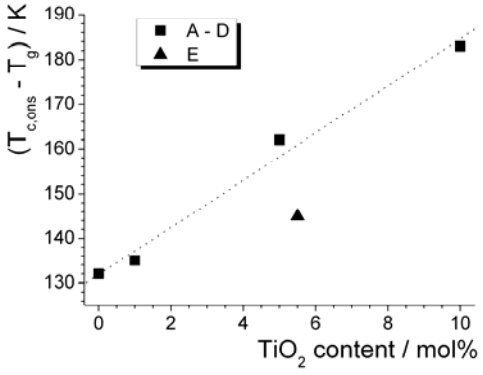

Figure 4: Processing window (crystallisation onset, $T_{c,ons}$, minus glass transition temperature, T_g) *vs*. TiO_2 content in mol%. The error is less than the size of the symbols. Dotted line represents linear regression of data for glasses A to D (R = 0.994).

For milled powder, DSC was run at different heating rates (5, 10, 15, 20 and 25 K/min); Fig. 5 shows the resulting curves for glass A. Fig. 6 is an Arrhenius plot of the dependencies of the crystallisation onset temperature ($T_{c,ons}$) *vs*. heating rate. T_g and $T_{c,pk}$ were plotted in analogous fashion (not shown). From the slopes of the straight lines, activation energies (E_a) for viscous flow (E_{Tg}) and crystallisation were calculated (Fig. 7) [13,14]. Activation energy for crystallisation increases shows a maximum for glass C (5 mol% TiO_2). TiO_2-free glass A shows the highest activation energy for viscous flow (E_{Tg}).

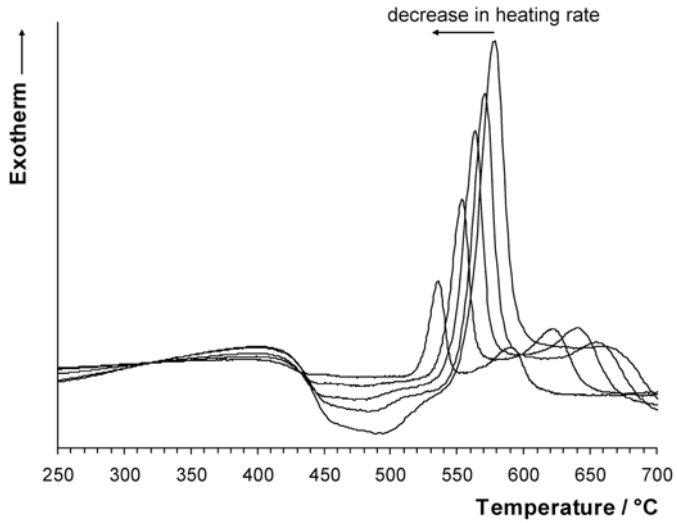

Figure 5: DSC curves of glass A obtained using heating rates of 5, 10, 15, 20 and 25 K/min. The highest temperature peak is for the highest heating rate and so on.

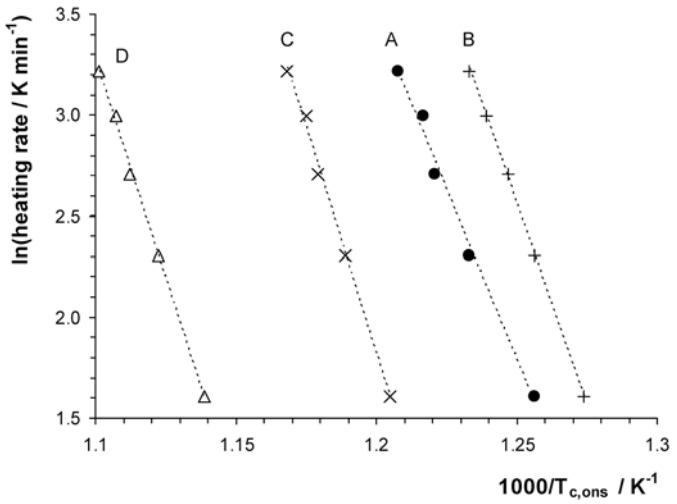

Figure 6: Arrhenius plot of the dependencies of crystallisation onset temperature ($T_{c,ons}$) for glasses A to D.

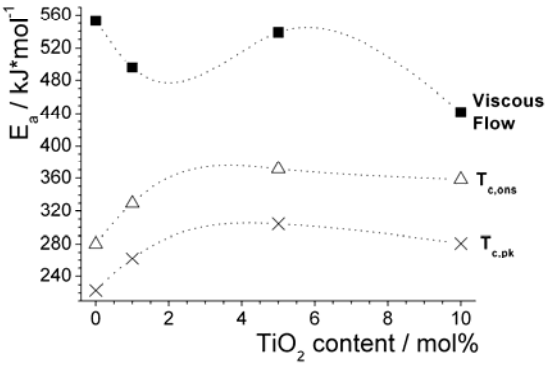

Figure 7: Activation energies for viscous flow, $T_{c,ons}$ and $T_{c,pk}$ *vs*. TiO_2 content in mol% for glasses A to D. The error is less than the size of the symbols. (Lines are drawn as a guide to the eye.)

For all glass compositions, $T_{c,ons}$ and $T_{c,pk}$ were lower for milled glass than for glass frit, which indicates surface crystallisation. Surface crystallisation is also found on heat-treated glass monoliths (Fig. 8).

Table 2: Glass transition (T_g), crystallisation onset ($T_{c,ons}$) and crystallisation peak ($T_{c,pk}$) temperatures and processing window ($T_{c,ons}$-T_g) from DSC traces (heating rate 10 K/min) run on frit and milled glass powder (shown in brackets).

Glass	T_g °C	$T_{c,ons}$ °C	$T_{c,pk}$ °C	Processing Window K
A	426 (421)	558 (525)	601 (537)	132 (104)
B	432 (417)	567 (523)	616 (534)	135 (106)
C	454 (444)	616 (568)	661 (579)	162 (124)
D	481 (473)	664 (618)	711 (643)	183 (145)
E	472 (470)	617 (599)	641 (612)	145 (129)

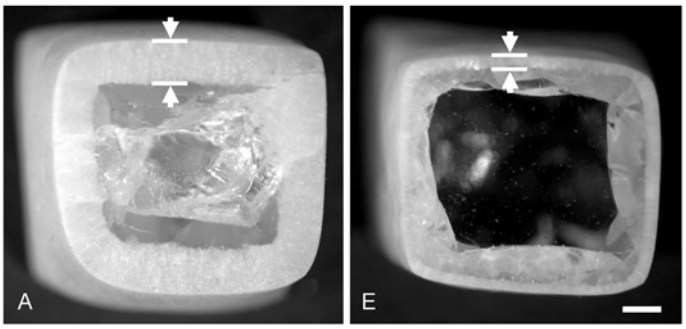

Figure 8: Glass monoliths of compositions A and E showing surface crystallisation after heat treatment for 30 min at 540°C (scale bar: 1 mm).

3.3 XRD and Raman

XRD patterns of heat-treated glass are shown in Fig. 9. Patterns of glasses A to C show peaks corresponding to calcium and magnesium pyrophosphate ($Mg_2P_2O_7$, $Ca_2P_2O_7$), glass E shows presence of calcium pyrophosphate and a mixed calcium magnesium pyrophosphate ($CaMgP_2O_7$) while glass D, which has the highest TiO_2 content, only shows presence of sodium titanium phosphate ($NaTi_2(PO_4)_3$). We cannot exclude the possibility that small amounts of additional phases (*e.g*. sodium-containing crystal phases in glasses A to C and E) are present as well, however, interpretation of small peaks in XRD was problemtatic.

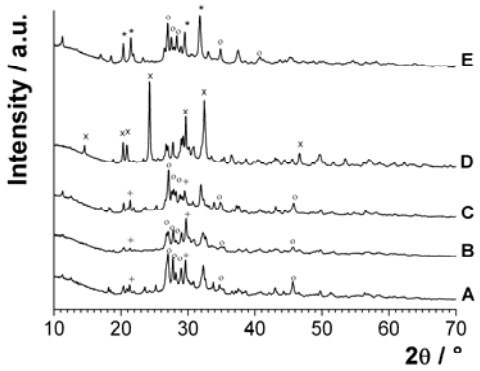

Figure 9: XRD pattern of heat-treated glasses A to D (37 mol% P_2O_5) and E (35 mol% P_2O_5). Crystal phases shown are: + $Mg_2P_2O_7$, ○ $Ca_2P_2O_7$, × $NaTi_2(PO_4)_3$ and * $CaMgP_2O_7$.

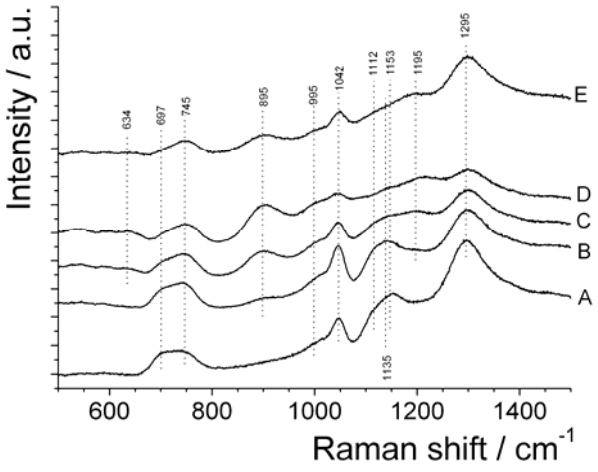

Figure 10: Raman spectra for glasses A to D (37 mol% P_2O_5) and E (35 mol% P_2O_5).

Raman spectroscopy (Fig. 10) showed increasing peaks at 636, 895 and 1195 cm^{-1}, peaks of decreasing intensity at 697, 1042, 1112, 1135, 1153 and 1295 cm^{-1}, while the intensity of the peak at 745 cm^{-1} stayed constant. According to Brow *et al*. the peak at 697 cm^{-1} can be assigned to symmetric stretch modes in bridging oxygens of Q^2 groups, while the peak

at 745 cm^{-1} is caused by those of Q^1 groups [15]. The peaks between 1000 and 1150 cm^{-1}, on the other hand, represent symmetric stretch modes of non-bridging oxygens in Q^1 (1042 cm^{-1}) and Q^2 units. The multiple peaks between 1100 and 1150 cm^{-1} can be explained by Q^2 groups interacting with different cations such as Ca^{2+}, Mg^{2+} or Na^+ [16]. The peak at 1295 cm^{-1} is likely to be an asymmetric partner of one of those Q^2 stretch modes [15]. The increasing peaks mentioned above can be assigned to titanate (TiO_6, 636 cm^{-1}) and titanyl (TiO_5, 895 cm^{-1}) units and a symmetric P-O stretch mode of phosphate interacting with titanium [15].

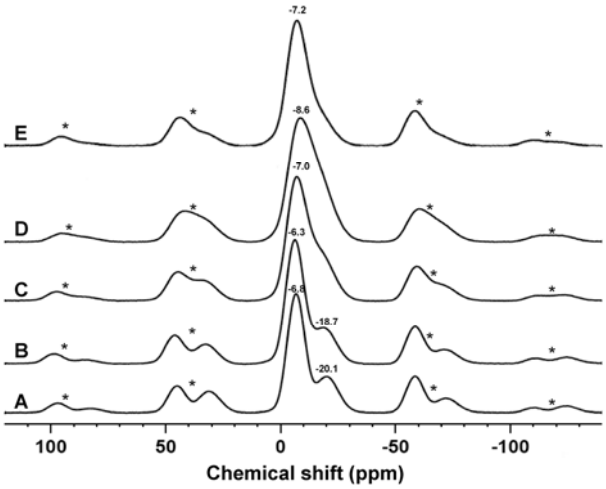

Figure 11: ^{31}P MAS NMR spectra of the glasses (*spinning side bands).

3.4 Solid-State MAS NMR

^{31}P MAS NMR of the glasses showed main peaks at chemical shifts in the range from -6.3 to -8.6 ppm, indicating Q^1 (pyrophosphate) species (Fig. 11). Spectra of glasses A and B showed another peak at -20.1 and -18.7 ppm (Q^2 metaphosphate units), while the main peaks of all other compositions showed a clear asymmetry, indicating presence of Q^2 units. No indication was found for orthophosphate being present in the structure. Absence of any sharp features suggests that crystallisation did not occur.

^{31}P MAS NMR of heat-treated glass E (Fig. 12) shows a broad peak with a maximum at about -7 ppm, a distinct shoulder at -14 ppm and a weak shoulder at about -2 ppm. Samples A to D (Fig. 12), on the other hand, clearly show presence of multiple sites, compared to the spectra of the glass. All four samples show multiple peaks in the range between -7 and -11 ppm and a broad shoulder between about -2 and -4 ppm. Samples A to C show a broad feature of lower intensity at about -20 ppm, while sample C shows an additional shoulder at -14 ppm. Of all five compositions, only sample D gives a distinct peak at -27 ppm and a broad, weaker peak at about -22 ppm.

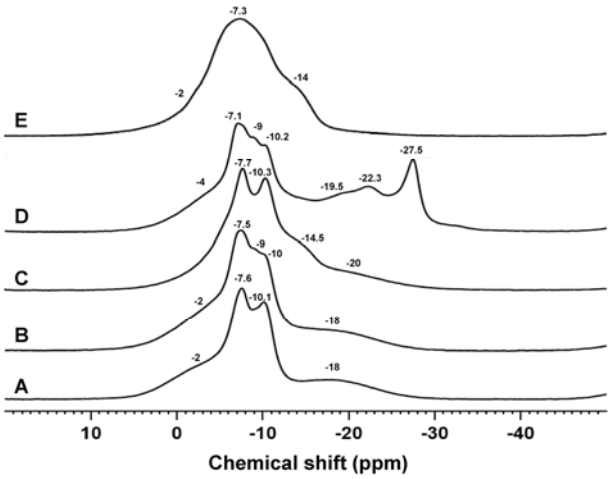

Figure 12: ^{31}P MAS NMR spectra of heat-treated glasses (*spinning side bands).

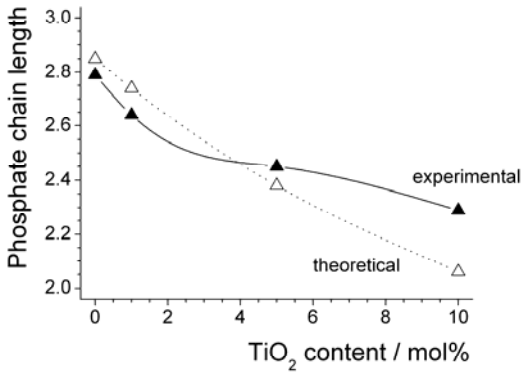

Figure 13: Experimental and theoretical phosphate chain lengths. Experimental data is based on deconvolution of ^{31}P MAS NMR data assuming presence of Q^1, Q^1(Ti) and Q^2 units. (Lines are drawn as a guide to the eye.)

4. Discussion

With increasing TiO_2 content transition and crystallisation temperatures increase and processing of the melt improved as the processing window increased significantly.

Activation energy for crystallisation increases with addition of TiO_2, showing a maximum for glass C (5 mol% TiO_2). Activation energy for viscous flow (E_{Tg}), on the other hand, decreases with addition of TiO_2, showing minima for glasses B (1 mol% TiO_2) and D (10 mol% TiO_2). This suggests that TiO_2-containing phosphate invert glasses are less likely to crystallise during processing and also sinter more readily, which is important for *e.g.* fabrication of porous scaffolds [17], where viscous flow sintering is desirable, and for fibre drawing [18].

As titanium is an intermediate oxide according to Dietzel [19] the influence of TiO_2 could be explained by either Ti going into the backbone of the glass network (*i.e*. acting as a network former) or by Ti acting as a network modifier with Ti^{4+} units acting as ionic crosslinks between phosphate units.

To identify the structural role of TiO_2 in this glass system and to understand its role in stabilising the glass network, Raman and ^{31}P MAS NMR experiments were performed. ^{31}P NMR spectra for the TiO_2-free glass (A) show two distinct peaks at -6.8 and -20.1 ppm, corresponding to Q^1 and Q^2 units, respectively. For increasing amounts of TiO_2 the Q^2 peak moves towards less negative chemical shifts (towards 0 ppm); for TiO_2 concentrations of 5 mol% and above (glasses C to E) only a shoulder is visible. Deconvolution of the spectra assuming presence of two peaks (Q^1 and Q^2) only, gave increasing chain length with increasing TiO_2 content (Table 3); however, no matter if TiO_2 acts as a network former or modifier, we would not expect the number of Q^2 units to increase, and deconvolution of NMR results should reflect this.

Table 3: Results for deconvolution of ^{31}P MAS NMR spectra assuming presence of Q^1 and Q^2 units only ($\overline{n}_{exp}$: experimental chain length).

	Q^1			Q^2			
Glass	Peak position (ppm)	Linewidth (ppm)	Proportion (%)	Peak position (ppm)	Linewidth (ppm)	Proportion (%)	$\overline{n}_{exp}$
A	-6.66	8.88	71.8	-20.23	11.63	28.2	2.79
B	-6.13	9.10	72.0	-18.95	12.26	28.0	2.78
C	-6.33	8.96	45.8	-14.29	17.29	54.2	4.36
D	-7.02	9.42	28.7	-13.48	17.45	71.3	6.98
E	-6.59	8.81	45.9	-11.5	17.99	54.1	4.35

Brow *et al*. discussed the presence of titanate (octahedral TiO_6) and titanyl (tetragonal pyramidal TiO_5) units when interpreting Raman spectra of P_2O_5-CaO-TiO_2 glasses, suggesting these units terminate the phosphate chains [15]. According to Brow *et al*., the TiO_x-units showed Raman shifts of 610 to 634 cm^{-1} (TiO_6) and 900 to 930 cm^{-1} (TiO_5) [15]. Raman spectra of glasses in our system show a peak of increasing intensity at about 895 cm^{-1}, which can be explained by formation of TiO_5 units with increasing TiO_2 concentration. On the other hand, only a faint peak is visible at 634 cm^{-1} for the glasses with higher TiO_2 content, suggesting that in our system titanium is present primarily as TiO_5 instead of TiO_6.

Table 4: Results for deconvolution of ^{31}P MAS NMR spectra assuming presence of Q^1, Q^1(Ti) and Q^2 units.

	Q^1			Q^1(Ti)			Q^2		
Glass	Peak	Linewidth	Proportion	Peak	Linewidth	Proportion	Peak	Linewidth	Proportion

	position			position			position		
	(ppm)	(ppm)	(%)	(ppm)	(ppm)	(%)	(ppm)	(ppm)	(%)
A	-6.66	8.88	71.8	n/a	n/a	n/a	-20.23	11.63	28.2
B	-6.5	8.88	74.6	-14.0	6.0	1.3	-19.5	10.0	24.1
C	-6.5	9.0	60.6	-14.1	10.0	21.2	-20.0	11.0	18.2
D	-6.6	9.5	37.6	-13.0	13.0	49.8	-21.0	10.0	12.6
E	-6.5	10.0	72.2	-14.1	10.0	17.5	-20.0	11.0	10.4

If these TiO_5 units terminate phosphate chains, they could be affecting the chemical shift of Q^1 chain end units. We therefore deconvoluted ^{31}P MAS NMR spectra again, this time accounting for the presence of an additional Q^1(Ti) peak as suggested by Montagne *et al*. [20] and Abrahams *et al*. [21], with the position of the Q^1 peak staying constant at about -6.5 ppm (Table 4). In this case, the chain length (*i.e*. the number of phosphate units per phosphate chain) decreases slightly with increasing TiO_2 content (Fig. 13). Brow *et al*. also noted a depolymerisation of the phosphate network, *i.e*. changes from a Q^2 metaphosphate to a Q^1 pyrosphosphate, with increasing TiO_2 content [15]. In their glass system, however, this depolymerisation is likely to be caused by a reduction in P_2O_5 content as well as TiO_2 addition, as TiO_2 was substituted for $Ca(PO_3)_2$, and an increase in TiO_2 concentration therefore simultaneously reduces the phosphate content. We see a similar effect for glass E, which contains 35 instead of 37 mol% TiO_2 (glasses A to D). Although glasses C and E are relatively similar in composition, the structure of glass E contains more Q^1 and less Q^2 units than the one of C, resulting in shorter phosphate chains and lower network connectivity (Table 5).

Table 5: Theoretical and experimental average chain length ($\bar{n}$) and network connectivity (NC); experimental values based on deconvolution of ^{31}P MAS NMR spectra assuming presence of Q^1, Q^1(Ti) and Q^2 units.

Glass	NC_{theor}	NC_{exp}	$\bar{n}_{theor}$	$\bar{n}_{exp}$
A	1.30	1.28	2.85	2.79
B	1.27	1.24	2.74	2.64
C	1.16	1.18	2.38	2.45
D	1.03	1.13	2.06	2.29
E	0.99	1.10	1.97	2.23

For glasses A to D, where phosphate content is kept fixed at 37 mol%, network connectivity and average chain length decrease with increasing TiO_2 content (Fig. 13), due to TiO_2 being more disruptive than CaO, MgO or Na_2O. One TiO_2 turns two BO's into four non-bridging oxygens (NBO), in contrast to *e.g*. CaO, which only causes formation of two NBO's from one BO. This agrees with our Raman results, which show a decrease in intensity of peaks related to Q^2 units. The decrease in intensity of Q^1 peaks can be explained by the formation of Q^1(Ti) species. Brow *et al*. described

formation of peaks in the range from about 850 to 1300 cm^{-1} with increasing TiO_2 content, which they assigned to P-O modes associated with developing Ti-O-P bonds [15], and we see a developing peak at 1195 cm^{-1} with increasing TiO_2 content.

Our results suggest that in the glass system studied titanium is acting as a network modifier, with Ti^{4+} crosslinking the phosphate units. As expected, this crosslinking is much stronger than that by Ca^{2+}, Mg^{2+} or Na^{+} and impedes crystallisation as well as chain hydration, which was shown to be the mechanism by which phosphate glasses dissolve [12].

XRD and ^{31}P MAS NMR or heat-treated samples show mostly presence of pyrophosphates, which is to be expected of glasses in the pyrophosphate composition range. ^{31}P MAS NMR spectra of the heat-treated samples (Fig. 12) demonstrate a significant increase in structural order compared to the untreated glasses. This is consistent with the phases identified on XRD patterns. XRD of heat-treated sample D showed sodium titanium phosphate, $NaTi_2(PO_4)_3$, as the main crystal phase, so the peak at -27 ppm might be caused by that phase. We were not able to find literature on the chemical shift of sodium titanium phosphate; however, according to MacKenzie and Smith [22] sodium zirconium phosphate, $NaZr_2(PO_4)_3$, gives a chemical shift of -24 ppm, and as we expect the chemical shift of $NaTi_2(PO_4)_3$ to be in a similar range, we assign the peak at -27 ppm to that phase. Calcium pyrophosphate, which according to XRD is present in heat-treated samples A to C as well as in E gives peaks at chemical shifts of about -8 and -10 ppm (α-$Ca_2P_2O_7$), while β-$Ca_2P_2O_7$ gives two additional peaks at -6 and -9 ppm [22]. Magnesium pyrophosphate gives peaks at chemical shifts of -13 and -20 ppm [22]. We therefore assign the peaks in the range between -7 and -11 ppm to $Ca_2P_2O_7$ and the broad peak at -20 ppm as well as the shoulder at -14 ppm to $Mg_2P_2O_7$. These results are in agreement with the findings by Dias *et al*. [23], who produced phosphate glass ceramics in the system $37P_2O_5$-45CaO-5MgO-$13TiO_2$ (mol%), which is very similar to our system but sodium-free, and they observed that α- and β-$Ca_2P_2O_7$ were the first crystal phases to appear during heat treatment. They also found calcium titanium phosphate, $CaTi_4(PO_4)_3$, and titanium pyrophosphate, TiP_2O_7. These results suggest that high TiO_2 concentrations are necessary for titanium to be incorporated into a crystal phase. We were unable to identify any sodium-containing phases in heat-treated samples A to C or E in XRD, but we cannot completely exclude its presence. Sodium pyrophosphate, $Na_4P_2O_7$ gives chemical shifts in ^{31}P MAS NMR of about 1.6 and 2.5 ppm. Our NMR spectra show a very broad shoulder in that range, which makes it difficult to assign phases, but it could also suggest presence of small amounts of sodium pyrophosphate. The fact that sodium phosphate in glasses A to C and E, if at all, only is present in small amounts might suggest that pyrophosphate has a preference for two-valent cations such as Ca^{2+} or Mg^{2+}.

Addition of TiO_2 is known to decrease glass solubility [15,24]. This can be explained by both Ti^{4+} providing improved cross-linking of the phosphate units compared to Ca^{2+}, Mg^{2+} and Na^{+}. In addition, addition of TiO_2 slightly disrupts the glass network as described above. Hydration energy in phosphates decreases for $Q^2 > Q^1 > Q^0$ (hence the hydrolytic stability of apatites) and thus the disrupting effect of TiO_2 also reduces solubility by increasing the relative amount of Q^1 species compared to Q^2 species. Our results also show that with increasing TiO_2 content in the glass by constant network modifier to P_2O_5 ratio (glasses A to D) the relative amount of network modifiers leached from the glass increases while the relative amount of phosphate decreases. This, again, can be explained by increased cross-linking of the phosphate units through Ti^4, which results in an increased hydrolytic stability of the phosphate units, while network modifier cations are still leached out of the glass.

5. Conclusion

Phosphate invert glasses with 37 mol% P_2O_5 show an increase in activation energy for crystallisation with increasing TiO_2 content, resulting in an increased processing window (up to 183 K) which facilitates sintering and fibre drawing. Deconvolution of ^{31}P MAS NMR and calculation of network connectivity and average chain lengths suggest that Ti is acting as a network modifier with Ti^{4+} units acting as ionic crosslinks between phosphate units thereby impeding crystallisation as well as chain hydration and subsequent chain dissolution.

References

[1] G. Walter, J. Vogel, U. Hoppe, P. Hartmann. J Non-Cryst Solids 296 (2001) 212.

[2] J. R. van Wazer. Phosphorus and its compounds. New York: Interscience; 1958.

[3] J. Vogel, P. Wange, S. Knoche, C. Rüssel. Glass Sci Technol 77 (2004) 82.

[4] D. S. Brauer, C. Rüssel, J. Kraft. Journal of Non-Crystalline Solids 353 (2007) 263.

[5] T. Kasuga, Y. Hosoi, M. Nogami, M. Niinomi. Journal of the American Ceramic Society 84 (2001) 450.

[6] P. Wange, J. Vogel, S. Knoche, C. Rüssel. Glass Sci Technol 77 (2004) 172.

[7] T. Kasuga, Y. Abe. Journal of Non-Crystalline Solids 243 (1999) 70.

[8] L. L. Hench. Journal of Materials Science: Materials in Medicine 17 (2006) 967.

[9] H. E. Kissinger. Analytical Chemistry 29 (1957) 1702.

[10] D. Massiot, F. Fayon, M. Capron, I. King, S. Le Calve, B. Alonso, et al. Magnetic Resonance in Chemistry 40 (2002) 70.

[11] R. Hill. Journal of Materials Science Letters 15 (1996) 1122.

[12] B. C. Bunker, G. W. Arnold, J. A. Wilder. J Non-Cryst Solids 64 (1984) 291.

[13] I. Avramov, C. Tzvetkova, T. Vassilev. Journal of Non-Crystalline Solids 355 (2009) 23.

[14] I. Avramov, T. Vassilev, I. Penkov. Journal of Non-Crystalline Solids 351 (2005) 472.

[15] R. K. Brow, D. R. Tallant, W. L. Warren, A. McIntyre, D. E. Day. Physics and Chemistry of Glasses 38 (1997) 300.

[16] M. A. Karakassides, A. Saranti, I. Koutselas. Journal of Non-Crystalline Solids 347 (2004) 69.

[17] D. S. Brauer, C. Rüssel, S. Vogt, J. Weisser, M. Schnabelrauch. Journal of Biomedical Materials Research Part A 80A (2007) 410.

[18] D. S. Brauer, C. Rüssel, S. Vogt, J. Weisser, M. Schnabelrauch. Journal of Materials Science: Materials in Medicine 19 (2008) 121.

[19] A. Dietzel. Z Elektrochem Angew Phys Chem 48 (1942) 9.

[20] L. Montagne, S. Daviero, G. Palavit. Chemistry of Materials 15 (2003) 4709.

[21] I. Abrahams, E. Hadzifejzovic, J. R. Dygas. Dalton Transactions 19 (2004) 3129.

[22] K. J. D. MacKenzie, M. E. Smith. Multinuclear solid-state NMR of inorganic materials. Amsterdam: Pergamon, Elsevier Science; 2002.

[23] A. G. Dias, J. M. S. Skakle, I. R. Gibson, M. A. Lopes, J. D. Santos. Journal of Non-Crystalline Solids 351 (2005) 810.

[24] M. Navarro, M. P. Ginebra, J. Clément, S. Martinez, G. Avila, J. A. Planell. J Am Ceram Soc 86 (2003) 1345.